Journal Name

ARTICLE TYPE

Cite this: DOI: 10.1039/xxxxxxxxxx

Supplementary Information: Elastic cavitation and fracture via injection†

Shelby B. Hutchens,*[a] Sami Fakhouri,[b‡] and Alfred J. Crosby*[b]

Received Date
Accepted Date

DOI: 10.1039/xxxxxxxxxx

www.rsc.org/journalname

1 Equilibrium Stretch Ratio

The initial equilibrium void size, $\Lambda_{eq} = A/A_0$ may be calculated from $P_{lp} + P_{elas} = 0$ corresponding to the equilibration of surface tension and elastic restoring force. Since $P = -\partial F/\partial V$, non-dimensionalizing F (free energy) by μA_0^3 and V (volume) by A_0^3 allows us to write

$$\frac{\partial F_{lp}/\mu A_0^3}{\partial a/A_0} + \frac{\partial F_{elas}/\mu A_0^3}{\partial a/A_0} = 0 \tag{S1}$$

The expression for the surface free energy is $F_{lp}/(\mu A_0^3) = 4\pi(a/A_0)^2(\gamma/\mu A_0)$. The strain energy in the elastomer F_{elas} is calculated as in Zhu *et al.* [1]

$$\frac{F_{elas}}{\mu A_0^3} = 4\pi\left(\left(\frac{a}{A_0}\right)^3 - 1\right)\int_1^{a/A_0} \frac{\lambda^2 W(\lambda)}{\mu(\lambda^3-1)^2} d\lambda, \tag{S2}$$

where W is the free energy function for the material model chosen. For a neo-Hookean solid, substituting the derivatives of the expressions for the free energy into Eq. S1 and noting that we are solving for what we are calling the initial void size A, yields

$$5\left(\frac{A}{A_0}\right)^4 + 4\frac{\gamma}{\mu A_0}\left(\frac{A}{A_0}\right)^3 - 4\left(\frac{A}{A_0}\right)^3 - 1 = 0. \tag{S3}$$

The second term in this equation can be re-written as $4\frac{\gamma}{\mu A_0}\left(\frac{A}{A_0}\right)^4$ yielding an equation that can be solved for the equilibrium stretch ratio $\Lambda_{eq} = A/A_0$ as a function of the parameter $\gamma/\mu A$.

$$\left(5 + 4\frac{\gamma}{\mu A}\right)\Lambda_{eq}^4 - 4\Lambda_{eq}^3 - 1 = 0 \tag{S4}$$

Λ_{eq} is the real solution between zero and one. In the case of the modified Yeoh model (Eq. 7) the expression is non-linear (involving $\log\Lambda_{eq}$).

Accounting for the initial equilibrium stretch ratio enables replication of the distinctive pressure versus applied compression observed experimentally (Fig. 1). In other words, relative pressure at the onset of compression is zero as in Figure S1. Additionally, bubble stretch values at cavitation are greater than one corresponding to bubble growth prior to cavitation as seen experimentally.

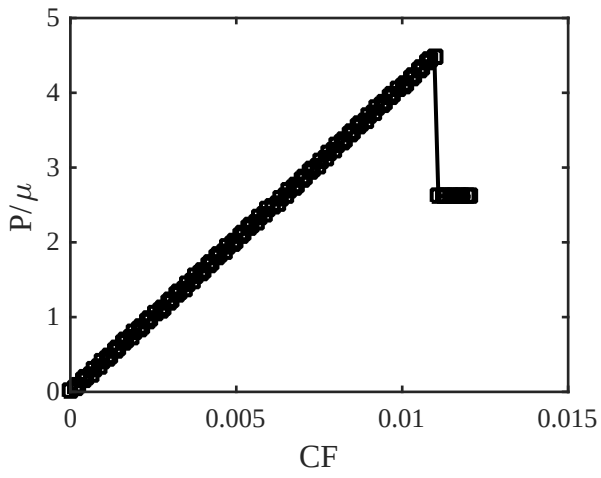

Fig. S1 As the syringe plunger is depressed, the compression fraction CF defined as $1 - V_c/V_{c0}$ increases. The increasing compression in the chamber leads to an increase in pressure. This figure illustrates the pressure-versus compression response for a gas mediated cavitation. (V_{c0} = 1 mL, μ = 250 Pa, A = 25 μm, γ = 27.7 mN/m, neo-Hookean)

[a] *Department of Mechanical Science and Engineering, University of Illinois Urbana-Champaign, Urbana, IL USA. Tel: 1-217-300-0412; E-mail: hutchs@illinois.edu*
[b] *Department of Polymer Science and Engineering, University of Massachusetts Amherst, Amherst, MA USA. Tel: 1-413-577-1313; E-mail: crosby@mail.pse.umass.edu*
† Electronic Supplementary Information (ESI) available: Supplementary document. See DOI: 10.1039/b000000x/

2 Yeoh Constitutive Response

The modified Yeoh model (Eq. 7) was used to approximate strain hardening while still resulting in neo-Hookean behavior in the limit of zero strain hardening ($C_3/\mu \to 0$). As is apparent in Figure S2, increased strain hardening is observed for increased in C_3/μ although these are accompanied by a slight increase in stiffness at small strain. This increase in small stretch stiffness has little effect on P_c from fracture and a relatively small contribution to G, making it a useful constitutive relation due to the closed form for F_{elas} that can be achieved with this relation as compared to, for example, Gent's.

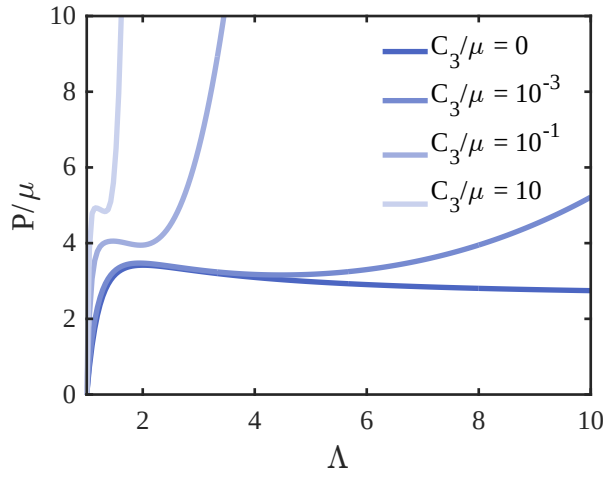

Fig. S2 Pressure-stretch response for a spherical void within an infinite elastic solid following the modified Yeoh constitutive model (Eq. 7). Decreasing saturation corresponds to decreasing stretch at hardening as determined by an increase in C_3/μ. ($\gamma/\mu A$ = 3)

3 Parametric Variation of Mechanism Maps in Both Gas and Incompressible Fluid Limits

Similar to Figure 3, increasing applied displacement can lead to an elastic cavitation or fracture event (Figure S3). Repeating this calculation over a range of parameters results in a mechanism map similar to Figure 5, only in this case we assume an incompressible fluid as the pressurizing liquid and a linear system compliance k to give Figure S4 for a neo-Hookean solid. Note that there is no empty space when an incompressible fluid is used; it is assumed that the applied volume V_{app} can always be large enough to cause the spring to reach P_c due to either elastic cavitation or fracture.

As discussed, the inseparability of two independent length scales, the needle size, A, and the elastocapillary length γ/μ necessitate the generation of a mechanism map for a series of one length scale by holding the other length scale constant. Figures S5 and S6 demonstrate the variation of the relationship between instability mechanisms for the gas and incompressible fluid limits, respectively.

Briefly, system compliance in the case of the incompressible fluid limit was measured by blocking the needle exit and loading the syringe/pressure sensor by displacing the syringe plunger using a syringe pump. Results of one of these experiments along with the linear fit of the observed slope are shown in Figure S7. This fit value is shown via a gray line in Figs. S4 and S6.

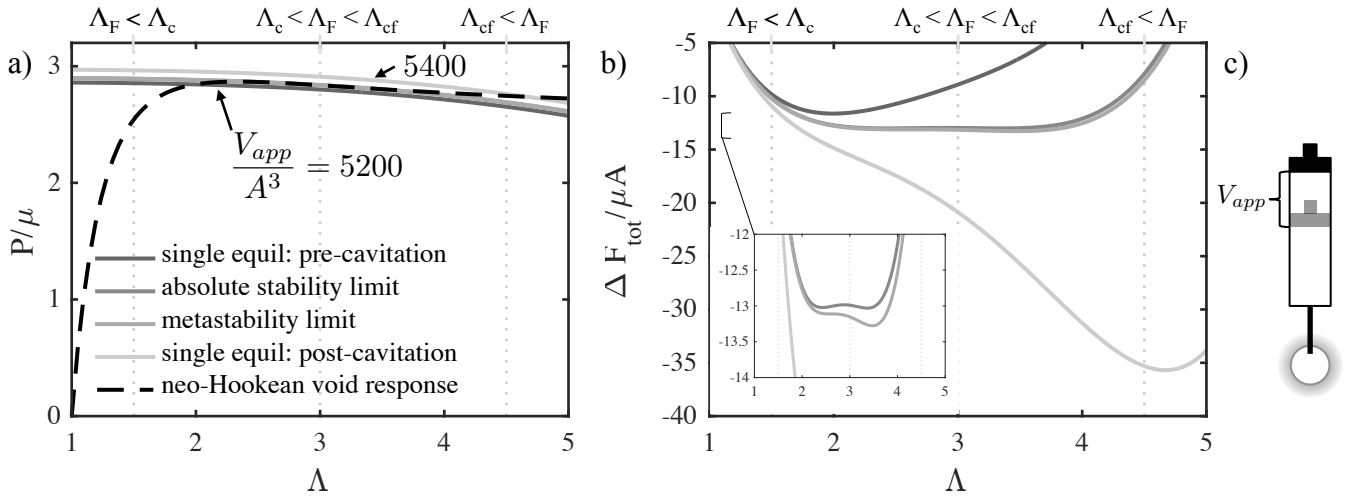

Fig. S3 a) Pressure-stretch response for a neo-Hookean void within an infinite elastic solid (dashed line). (A = 50 μm, μ = 250 Pa, γ = 27.7 mN/m) Overlays of decreasing saturation correspond to increasing displaced volume V_{app} (i.e., depressing the syringe) for compression levels reaching single, absolute, and meta- stability limits. ($k = 1.1$ kPa/μm, P_0 =1 atm) b) Free energy-stretch response for the combined void/syringe system plotted in a) illustrating the onset of absolute and meta-stability. ($\Delta F_{tot} = F_{tot}(\Lambda) - F_{tot}(1)$) c) Schematic illustrating the applied or displaced volume V_{app}.

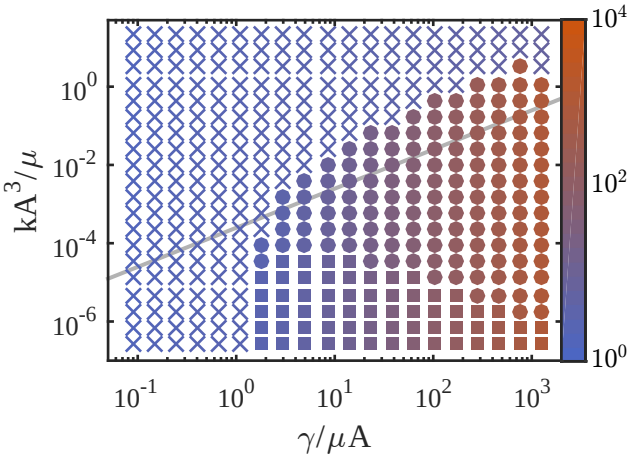

Fig. S4 Map detailing the mechanism leading to observation of a P_c during a CR experiment under the incompressible fluid assumption. '×' corresponds to fracture, '●' to cavitation, '■' to cavitation followed by fracture, and '★' to a negligible pressure drop during cavitation such that P_c is governed by fracture. The magnitude of P_c is shown via color gradient corresponding to the colorbar on the right. This map was generated assuming a constant needle radius of 50 μm, $G_c = 20\gamma$, $\gamma = 27.7$ mN/m (air-2-ethyl hexanol interface), and $P_0 = 1$ atm for a neo-Hookean solid. (Gray line corresponds to $k = 1.1$ kPa/μL.)

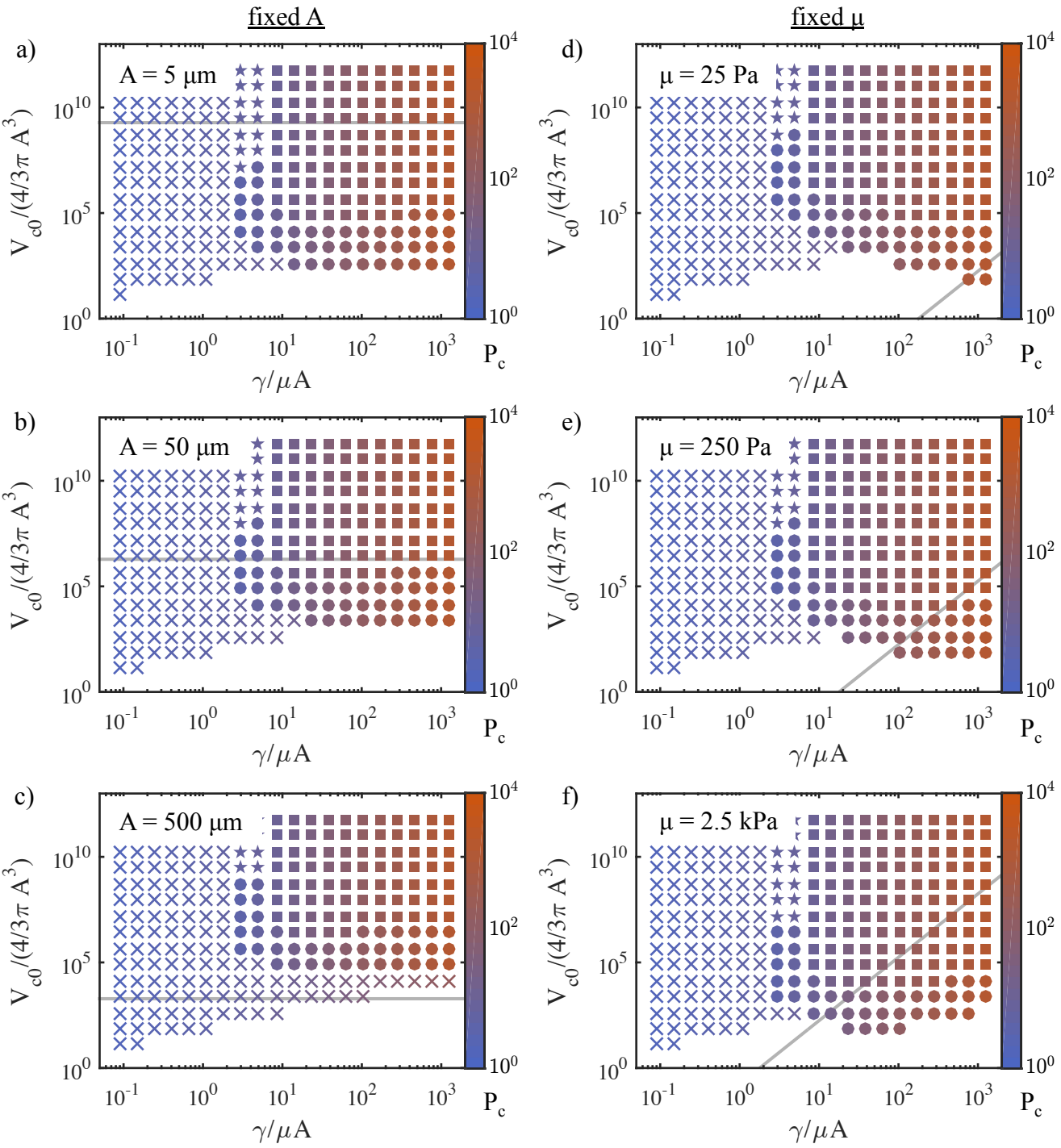

Fig. S5 Series of mechanism maps for the pressurizing gas case demonstrating length scale dependence for either fixed needle size (a-c) or fixed elastocapillary length, fixed μ, (d-f). The gray line in each figure corresponds to $V_{c0} = 1mL$. ($G_c = 20\gamma$, $\gamma = 27.7$ mN/m (air-2-ethyl hexanol interface), and $P_0 = 1$ for a modified Yeoh solid with $C_3/\mu = 0.01$.)

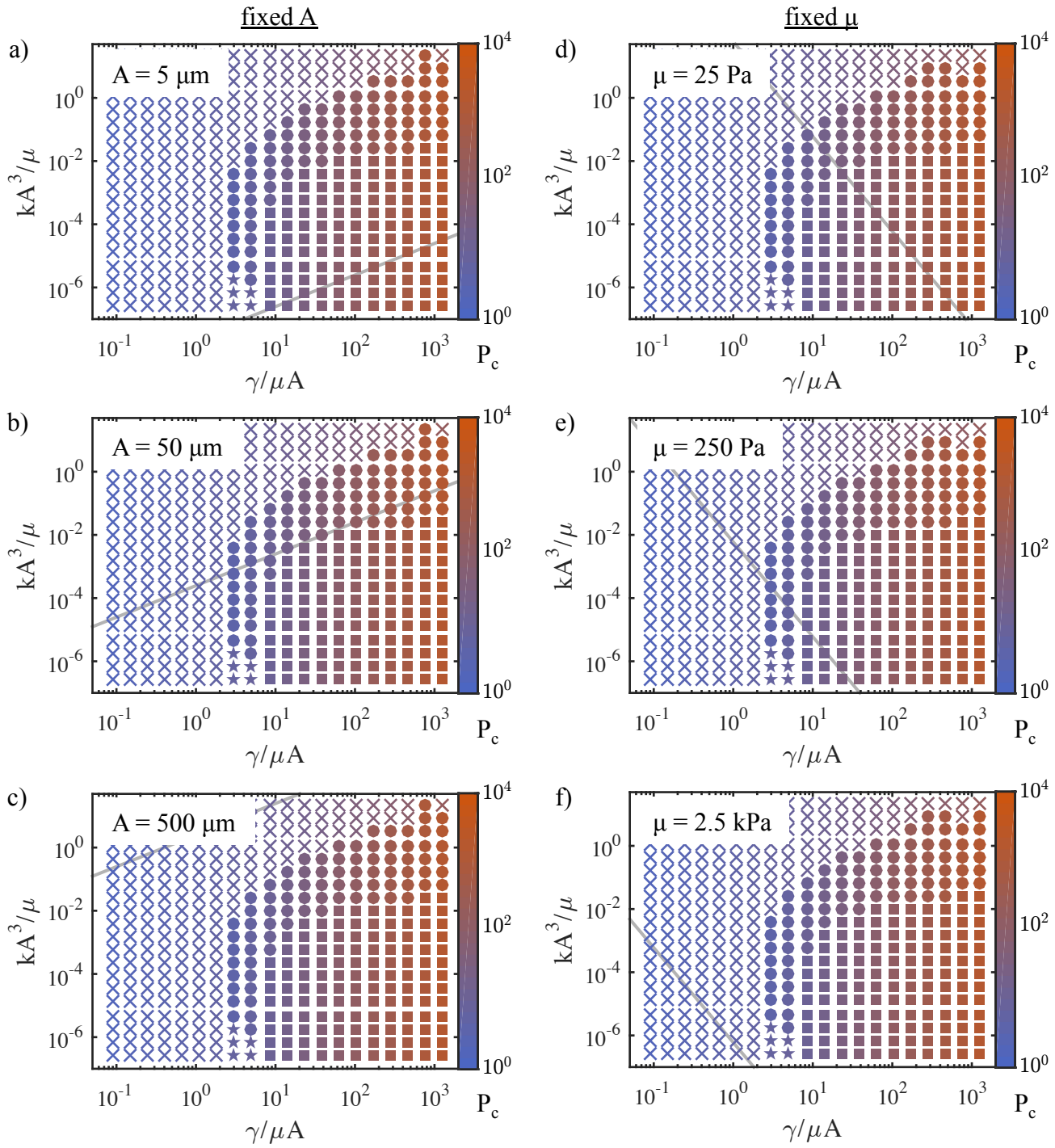

Fig. S6 Series of mechanism maps for the incompressible fluid/ finite system compliance case demonstrating length scale dependence for either fixed needle size (a-c) or fixed elastocapillary length, fixed μ, (d-f). The gray line corresponds to $k = 1.1$ kPa/μL. ($G_c = 20\gamma$, $\gamma = 27.7$ mN/m (air-2-ethyl hexanol interface), and $P_0 = 1$ for a modified Yeoh solid with $C_3/\mu = 0.01$.)

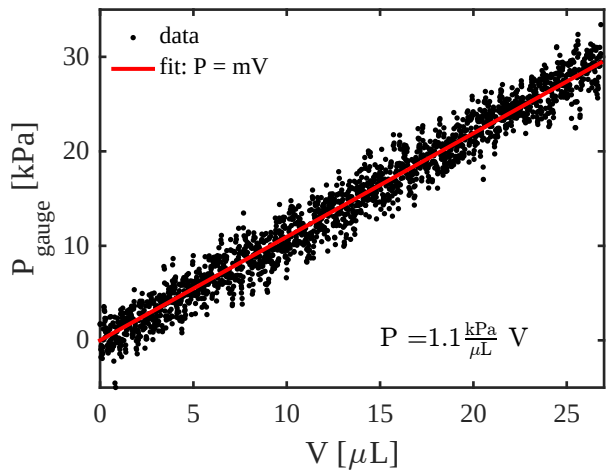

Fig. S7 Pressure increase with applied volume V_{app} for the closed syringe/pressure sensor system over a range of pressures exceeding those attained during triblock CR experiments.

4 Triblock Co-Polymer Gels

Triblock gels were prepared as a 7 wt% solution of PMMA-PnBA-PMMA with block lengths of 25, 116, and 25 kg/mol (Kuraray) dissolved in 2-ethyl-1-hexanol. The solution was covered and heated to 70°C for at least 1 hour (longer for the initial preparation) prior to allowing the solution to cool at room temperature (∼15 mL within a 20 mL glass vial). Samples were then brought up to temperature in a water bath monitored by a thermometer and allowed to equilibrate for at least 30 minutes. Each cavitation experiment was performed with the needle embedded approximately 2 cm below the sample surface as estimated by a ruler. A portion of the syringe was filled with water, leaving the needle and any remaining bubbles as the only air in the system. A volumetric flow rate of 50 μL/min was used to pressurize the sample as controlled with a syringe pump. The data gathered in this way are shown in Figure S8.

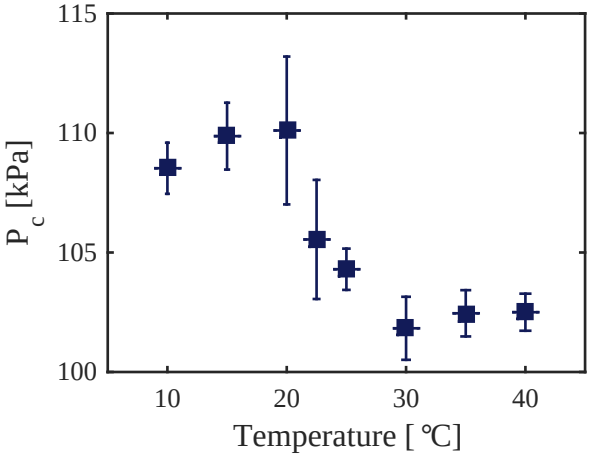

Fig. S8 Absolute P_c values for 7 wt% PMMA-PnBA-PMMA triblock gels using a 30 g stainless steel needle, ID: 106 μm, OD: 266 μm.

Rheological data (TA Instruments) was gathered using standard-size double cylinders in which the liquid solution was poured into the pre-heated, temperature controlled sample holder. Data, shown in Figure S9, were taken at varying frequencies and an oscillation strain of 5×10^{-5} .

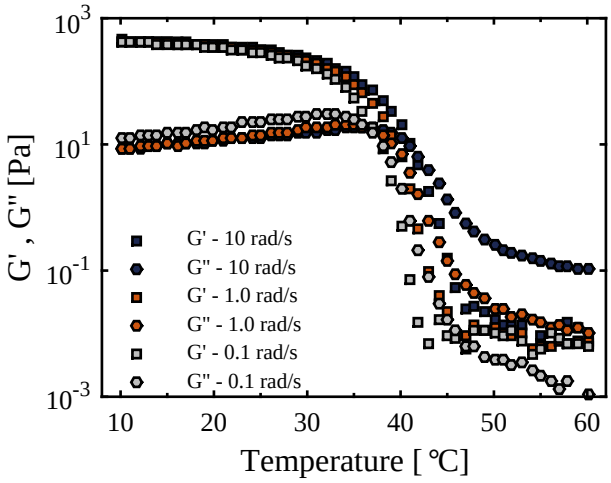

Fig. S9 Shear rheology data temperature sweeps for 7 wt%PMMA-PnBA-PMMA triblock gels at a range of .

5 Power Law Scaling of G_c

These scaling relation discussed here are direct extensions of those made by Kundu and Crosby[2] and apply to cross-linked gel systems. From classical gel mechanics, $\mu \sim \frac{kT}{b^3 N}\phi$ where k is Boltzman's constant, T is the temperature, b is the Kuhn length, N is the number of chain segments, and ϕ is the volume fraction of polymer. Following their arguments based on the Lake and Thomas[3] model for strain energy, G_c for a good solvent scales as $G_c \sim UN^{1/2}\phi^{7/8}/b^2$. For the PAAm gels characterized, contact mechanics found that $\mu \sim \phi^{2.3}$. Substituting this into the expression for μ, one obtains $N \sim \phi^{-1.3}$, which when substituted back into the expression for μ yields $\mu \sim \phi^{2.3}$. Similarly substituting N into G_c results in $G_c \sim \phi^{0.225}$. Combining these two dependences on volume fraction ϕ results in a power dependence:

$$G_c \sim \phi^{0.098}. \tag{S5}$$

Figure 7 demonstrates the effect of G_c scaling and strain hardening on P_c predictions for the case of the gas with a fixed needle radius. Similar behavior is observed when the elastocapillary length/μ is held constant as demonstrated in Figure S10 for an identical set of parameters.

6 Modulus and Fracture Energy Comparisons to Model Predictions

To determine the percent error of the cavitation equation predictions for modulus μ_{cav}, values were compared to μ obtained from shear rheology data at a frequency of 0.1 rad/s or less (triblocks and HSA organogels) or from contact mechanics (PAAm). The expression, whose results are plotted in Figure S11a is:

$$\%\text{Err} = \frac{\mu_{cav} - \mu}{\mu} \tag{S6}$$

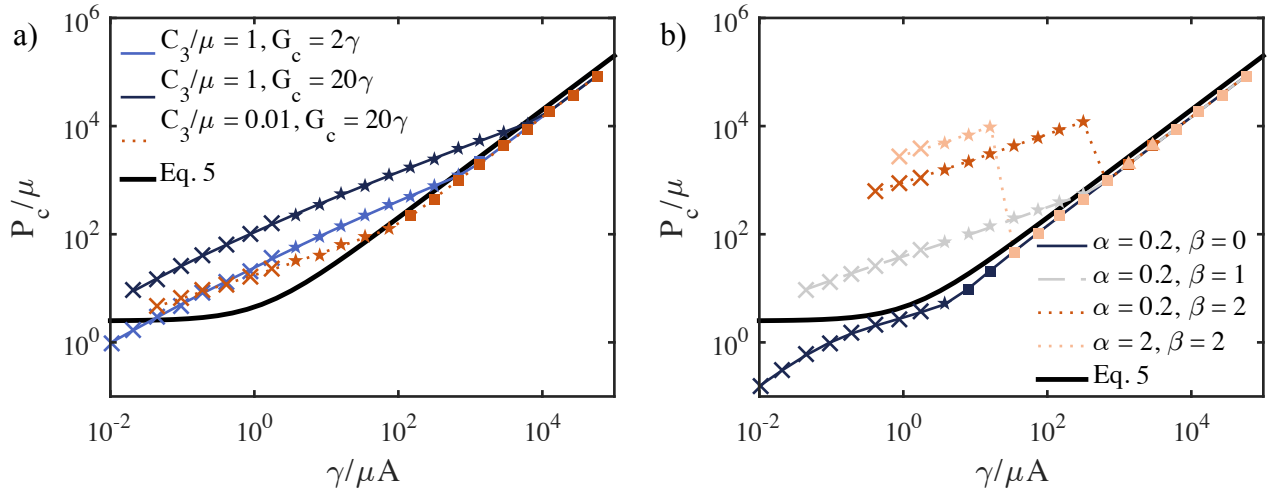

Fig. S10 Normalized P_c values predicted for varying constitutive behavior and G_c for a parameter series at constant modulus (varying needle radius). The cavitation equation (Eq. 5) is the black solid curve in both plots. a) Effect of increasing strain-hardening corresponding to an increase in C_3/μ. Light and dark blue curve illustrates associated effect of increases in G_c (increased P_c) combined with strain hardening. ($\mu = 500$ kPa, $V_{c0} = 1$ mL, $\gamma =$ 27.7 mN/m) b) Predictions after incorporation of the power law dependence for G_c (Eq. 8). In contrast to Figure 7b, increases in α tend to shift the P_c within the fracture regime only slightly. Much larger increases in P_c are observed with increases in β. When μ is held constant, as in these plots, increases in β do not affect the slope within the fracture regime. ($\mu = 500$ kPa, $V_{c0} = 1$ mL, $\gamma = 27.7$ mN/m, C_3/μ = 0.01)

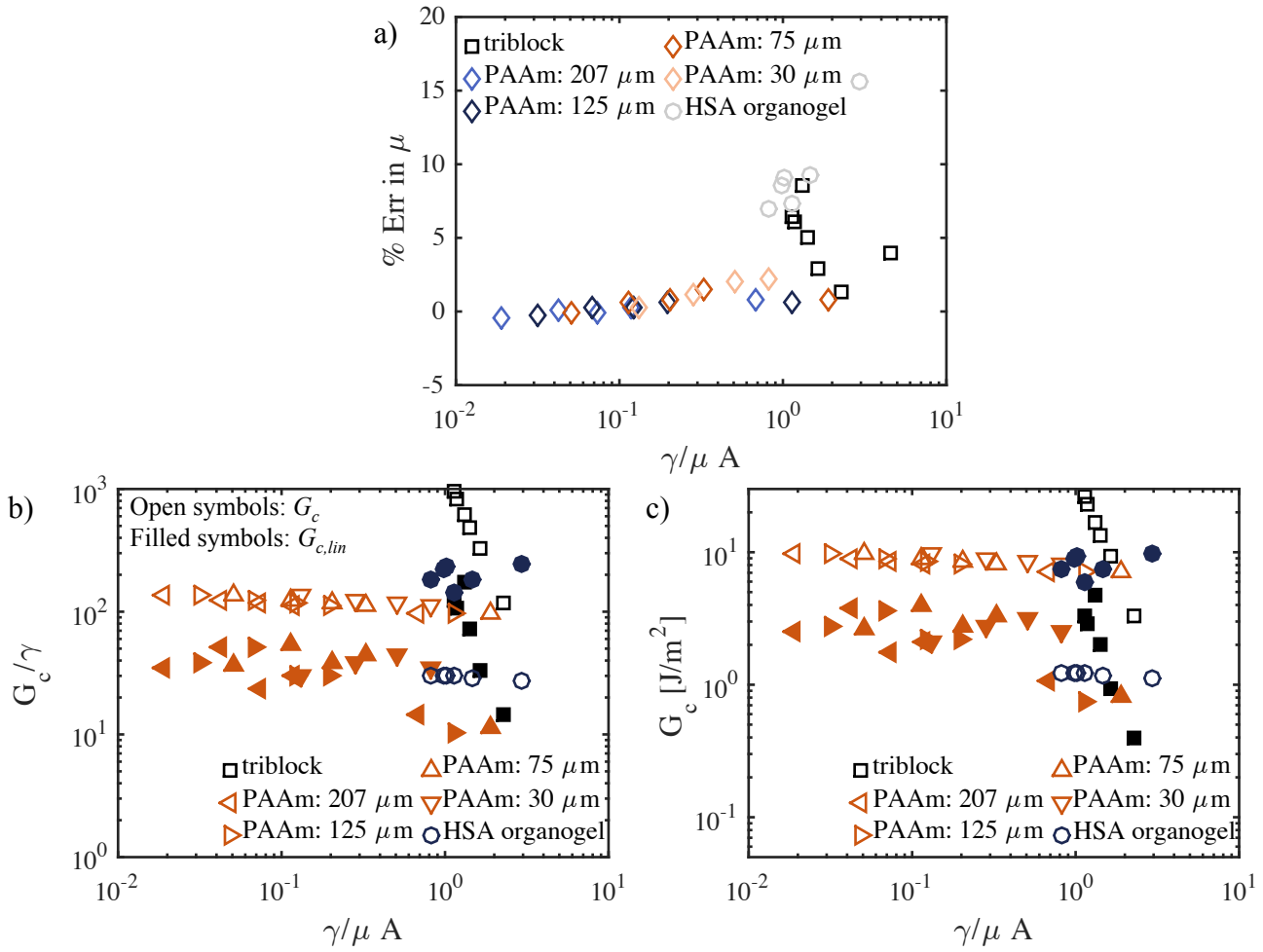

Fig. S11 a) Percent error (Eq. S6) in μ as predicted by the cavitation equation (Eq. 5) and compared to μ obtained using more standard techniques. b)-c) G_c (open symbols, Eq. 8) and $G_{c,lin}$ (closed symbols, Eq. 9) as a function of $\gamma/\mu A$ expressed relative to surface energy (b) and with units (c). The former is included in order to show fracture energy values relative to the minimum energy associated with the creation of two new surfaces at the tip of a crack, 2γ.

References

1 J. Zhu, T. Li, S. Cai and Z. Suo, *J. Adhes.*, 2011, **87**, 466–481.

2 S. Kundu and A. J. Crosby, *Soft Matter*, 2009, **5**, 3963.

3 G. J. Lake and A. G. Thomas, *Proc. R. Soc. Lond. A. Math. Phys. Sci.*, 1967, **300**, 108–119.